Earthquakes and Structures, *Vol. 28, No. 6 (2025) 507-520*
https://doi.org/10.12989/eas.2025.28.6.507

Development of an image-based automatic reinforcement modeling and inspection (I-ARMI) technique

Jaehee Choi[1], Kun-Ho E. Kim[2], Young K. Ju[3], Sanghee Kim*[4] and Donghyuk Jung**[3]

[1]*Department of Civil, Environmental and Architectural Engineering, Korea University, Seoul 02841, Korea*
[2]*Department of Civil and Environmental Engineering, University of Waterloo, Waterloo, ON, Canada N2L 3G1*
[3]*School of Civil, Environmental and Architectural Engineering, Korea University, Seoul 02841, Korea*
[4]*Department of Architectural Engineering, Kyonggi University, Suwon 16227, Korea*

(Received September 17, 2024, Revised April 16, 2025, Accepted April 18, 2025)

Abstract. Inspecting the accuracy of reinforcing bar placement in reinforced concrete (RC) structures is a critical procedure for ensuring the safety of structures. However, the current inspection methods are time-consuming and labor-intensive. Recent studies have been exploring the use of 3D scanners and depth cameras as inspection tools for reinforcing bars. Although there has been extensive research on bar length and spacing, limited numbers of studies have been carried on diameter detection, and they showed relatively low accuracy, especially for smaller bar diameters (D10 and D13). This study presents a photogrammetry-based automatic reinforcing bar information detection technique. By using readily accessible smartphones, images are acquired to generate 3D point clouds, and then automatic inspection procedures for bar diameter, length, and spacing are conducted. The efficacy of the proposed technique is experimentally investigated through the verification on laboratory-scale specimens (grid-type bar assembly and steel cage). It showed an accuracy of 97% in length and spacing the estimation of steel bars. Furthermore, it can effectively differentiate the diameter of D10 and D13 bars. This technique is expected to be utilized for accurate and rapid reinforcing bar placement inspections on construction sites.

Keywords: 3D modeling; image processing; photogrammetry; point cloud data; reinforcing bar inspection

1. Introduction

In construction of reinforced concrete (RC) structures, incorrect placement and/or missing of steel reinforcement, as opposed to structural drawings, can severely impact the quality of construction and, more importantly, the safety of the structural system, potentially leading to major accidents involving loss of life and property such as structural collapses (Hidayat *et al.* 2020, Chalioris *et al.* 2020, Nemutlu *et al.* 2021, Mahamid *et al.* 2024, Im *et al.* 2025). Therefore, inspecting the placement of reinforcing bars is a crucial procedure for ensuring the structural safety and constructability. Especially, the diameter and spacing of reinforcing bars significantly influence the strength and failure modes of RC structures. Before casting concrete, it is essential to scrutinize the accurate reinforcing bar placement by comparing it with structural drawings and checking the compliance with design codes and standards. In current practice, reinforcing bar inspection on construction sites is conducted mainly through visual inspection and manual measurements by several individuals. The assessment quality is likely to be subjective and highly dependent on personal experience and skill of the inspectors. This conventional method is time-consuming and difficult to achieve high accuracy (Wang *et al.* 2017). Realistically, it is nearly impossible for a limited number of inspectors to thoroughly inspect large-scale construction sites, making it difficult to acquire comprehensive information. Therefore, there is a growing need for automated techniques that provide accurate reinforcing bar information with reduced time and costs.

In response to this need, recent studies have been conducted on acquiring reinforcing bar information by analyzing images of reinforcing bars (Balbin *et al.* 2017, Shin *et al.* 2021). Techniques such as the Hough transform and Canny edge detection using computer vision (CV) and image processing have been applied to automate reinforcing bar information detection. However, existing research analyzing captured images relies on images taken from a limited perspective, making it difficult to analyze multidimensional characteristics of the bars such as bending and inclination. If the image shows only one side of the bars, it becomes challenging to assess the reinforcing bar information on the opposite side. Moreover, in 2D images, it is difficult to accurately identify overlaps or stacked configurations of bars, which can lead to discrepancies with the actual reinforcement situation. This can introduce errors in the assessment of the structural safety.

On the other hand, using 3D modeling to verify reinforcing bar information allows viewing bar layout from various angles, thus acquiring a wealth of information. Hence, various technologies have been developed to examine reinforcing bar placement based on 3D modeling techniques. Among many others, the 3D point cloud is the

*Corresponding author, Assistant Professor
E-mail: sanghee0714@kyonggi.ac.kr
**Corresponding author, Associate Professor
E-mail: jungd@korea.ac.kr

ISSN: 2092-7614 (Print), 2092-7622 (Online)

most representative method that shapes real objects with numerous points in 3D (X, Y, Z) coordinates. The quality of 3D point cloud data (PCD) can vary depending on the image resolution, shooting angle, and scan distance. Well-constructed 3D PCD can be utilized for reinforcing bar inspection (Luo *et al.* 2022). Techniques for implementing 3D models through PCD include 3D laser scanning, red green blue-depth (RGB-D) sensors, and photogrammetry. Laser scanning, in particular, is often used in 3D PCD for buildings and civil infrastructure due to its ability to acquire precise and detailed 3D PCD (Pleansamai and Chaiyasarn 2019, Cheng *et al.* 2023). However, a separate expensive piece of equipment, the laser scanner, is required, and in some cases, it is difficult to perform measurements on actual construction sites due to the need to secure space for equipment installation (Alaloul *et al.* 2021). While laser scanners can generate point clouds with mm-level accuracy under laboratory conditions, various factors such as laser wave reflection off object surfaces can cause significant modeling errors on actual construction sites (Shen *et al.* 2013). Kim *et al*. (2021) acquired PCD using a 3D laser scanner and measured the diameter and spacing of reinforcing bars based on machine learning. The distance detection between reinforcing bars showed high accuracy but the prediction for smaller-diameter bars (i.e., D10 and D13 bars) showed limitations with low accuracy. RGB-D sensors are less expensive and easier to measure than scanners, but they have the disadvantage of difficulty in acquiring accurate models in non-uniform lighting environments (Yuan *et al.* 2021). Other technologies like light detection and ranging (LiDAR) and RGB-D sensors have limitations in detecting reinforcing bar diameter, showing errors at the cm-level (Yuan *et al.* 2023). Meanwhile, photogrammetry is a technology which uses captured images acquired from digital cameras, smartphones, drones, and other image capture equipment, thus it is inexpensive and has high accessibility for data collection (Cavaco *et al.* 2019). Photogrammetry has been used to create 3D PCD, which are then converted to 2D images to automatically detect the length and diameter of reinforcing bars and the spacing between the bars (Qureshi *et al.* 2022). Previous research has proposed various methods for automatic detection of reinforcing bar information, and many studies have focused on acquiring the length and spacing of bars. However, a limited number of studies have been carried out on detecting the diameter of reinforcing bars (Kim *et al*. 2021).

This study presents a new image-based automatic reinforcement modeling and inspection (I-ARMI) technique which capitalizes on the benefits of photogrammetry. The proposed technique is capable of measuring the length and spacing of reinforcing bars, and especially the diameter of smaller-diameter bars (i.e., D10 and D13 bars) with the mm-level accuracy. To demonstrate the concept of I-ARMI technique, laboratory-level verification is carried out first for a small-scale reinforcing bar grid sample and then for an RC beam member. The current paper provides detailed descriptions on 1) the acquisition of high accuracy 3D PCD from a series of image frames, 2) the development of an algorithm for automatic reinforcing bar information detection, and 3) the validation of the proposed technique using reinforcing bar specimens.

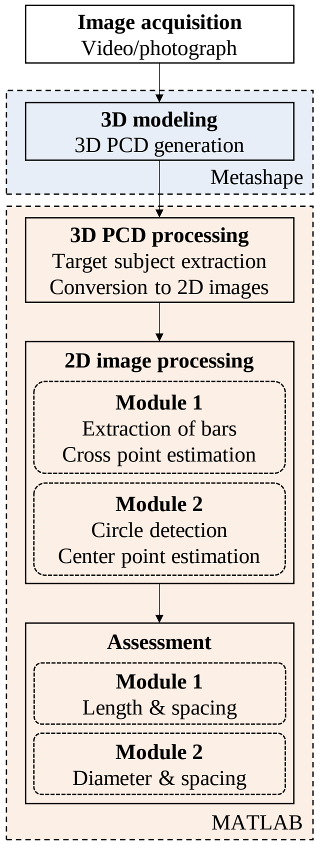

Fig. 1 Framework of I-ARMI technique

2. Development of a framework

Fig. 1 illustrates the overall framework of the I-ARMI technique established in this study. The framework consists of six stages: 1) image acquisition, 2) 3D modeling, 3) 3D PCD processing, 4) 2D image processing, and 5) data interpretation and assessment. Detailed explanations for each stage are provided in this section. The photogrammetry-based 3D modeling begins with acquiring images of a target subject. The 3D modeling approach adopted in a previous study (Qureish *et al.* 2022) is used in this study. 3D PCD created from the images are imported into MATLAB and transformed into 2D raster images for further processing. Two different analysis modules are developed depending on the type of needed information. After the analysis, the MATLAB software program automatically displays the length, diameter and spacing of reinforcing bars in the designated locations defined by a user.

2.1 Image acquisition and 3D modeling

Images of reinforcing bars can be obtained by taking photographs from various angles or by recording a video and extracting image frames. From a preliminary study, it was found that extracting frames from a video can accelerate the image acquisition process compared to taking

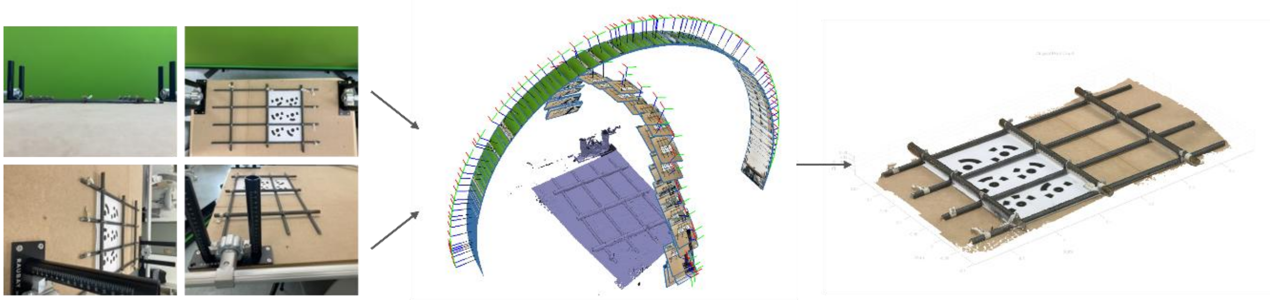

(a) Image (b) Photogrammetry (c) 3D PCD

Fig. 2 3D PCD generation from video-captured images

multiple photographs. In this study, as a low-cost video recording device, a 3rd-generation iPhone SE is used with a video resolution of 1920×1080 pixels at 60 frames/sec. Videos are shot to include all angles of the target subject, maintaining a distance of about 1 m between the subject and the camera. This distance is used to ensure the generation of a uniform distribution of point clouds and to keep the focus on the target subject rather than the background, and to avoid unfocused, blurry images during the subsequent frame extraction process. During video recording, markers are required for scaling of 3D PCD. Markers should be placed near the subject so that the images include both the target subject and the markers, allowing for the creation of a model that incorporates the markers.

For 3D modeling (i.e., generating of 3D PCD), Agisoft Metashape, a photogrammetry software program capable of generating 3D spatial data from digital images, is selected. When images are imported into Metashape, tie points are created by computing common features or locations within overlapped areas among adjacent images. Then, using ‘build mesh’ function, a 3D model is created, and a point cloud is built with a uniform point spacing of 1~5 mm. From coordinate directions and scale information defined by the markers, the model is created to match the actual dimensions of the subject. Using markers provided by Metashape enables the automatic recognition of the markers and the enhanced modeling accuracy. Fig. 2 depicts how 3D PCD can be constructed from images captured in a video for the reinforcing bar grid specimen.

2.2 3D PCD processing

2.2.1 Target subject extraction

3D point cloud data generated in Metashape were imported into MATLAB for further processing. The raw 3D PCD include not only the target subject (i.e., reinforcing bars) but also background elements such as the floor surface. Through plane detection process, unnecessary plane shape backgrounds are automatically detected and removed from the 3D model so that only the reinforcing bars remain. In MATLAB, to detect planes in the raw data, backgrounds are selected as a region of interest by setting reference vectors normal to the planes, using MATLAB’s built-in function, ‘pcfitplane’ which fits planes to 3D PCD. This function utilizes the M-estimator sample consensus (MSAC) algorithm, a variation of the random sample consensus (RANSAC) algorithm. The RANSAC algorithm is used to remove outliers that deviate abnormally from the distribution of variables in a dataset and to obtain the predicted homography matrix (Torr and Zisserman 2000). Both RANSAC and MSAC algorithms can control the probability (p) of selecting a sample entirely composed of inliers, and the quality of model is estimated by minimizing a cost function (C), the sum of squared error, in Eq. (1) and Eq. (2), respectively.

$$p = 1 - (1 - \alpha^m)^N \tag{1}$$

$$C = \sum_{i=1}^{m} \rho(e_i^2) \tag{2}$$

where α is the proportion of inliers in the dataset, m is the number of data points sampled per iteration, N is the number of iterations of the algorithm, ρ is the error function, and e_i is the error or residual of the i^{th} data point. The key difference between the two algorithms lies in $\rho(e^2)$ used to evaluate the model fit. If the threshold (T) between inlier and outlier is set too high, many solutions can have the equal values of C, increasing the likelihood of estimation errors. In RANSAC, the model is estimated simply by counting the number of inliers. In contrast, MSAC performs a more refined model evaluation, considering the magnitude of each point’s error as indicated in Eq. (3). This allows for more accurate estimations even in complex environments where inliers and outliers are mixed (Torr and Zisserman 2000). Fig. 3 illustrates the process of detecting and removing planes from the raw data, thereby extracting the reinforcing bars.

$$\rho(e^2) = \begin{cases} e^2 \text{if} e^2 < T^2 \\ T^2 \text{if} e^2 \geq T^2 \end{cases} \tag{3}$$

2.2.2 Conversion to 2D images

The 3D PCD have comprehensive and all-inclusive information on the target subject. However, for an efficient information acquisition needed for the inspection of reinforcing bars, the processing and analysis using 2D images can be more appropriate. Therefore, 3D PCD of reinforcing bars can be sliced at several locations of particular interest, and corresponding cross-sections are converted into 2D images. Depending on the type of needed information, 3D PCD can be cut in different directions. For example, Fig. 4 depicts the section cutting of the reinforcing bar grid specimen model by parallel and perpendicular

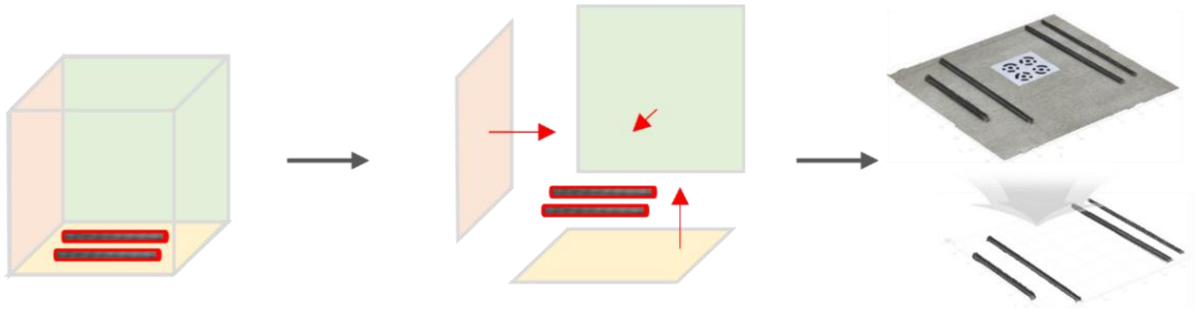

(a) 3D PCD generation (b) Plane detection (c) Reinforcing bar extraction

Fig. 3 Plane detection process

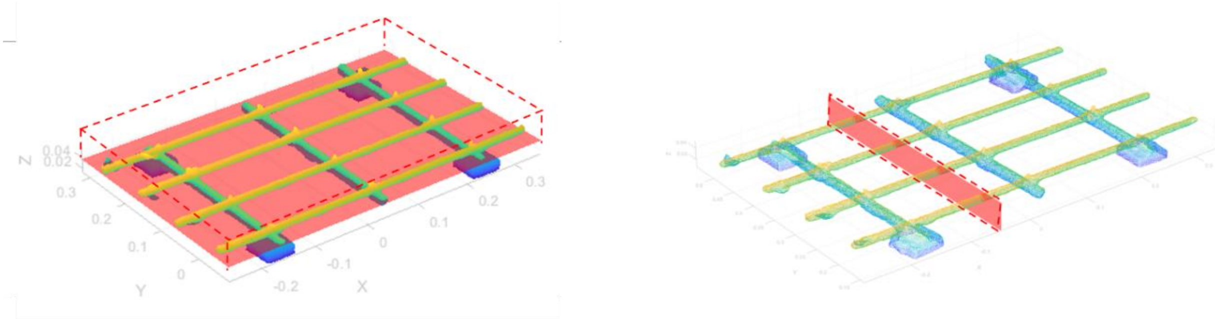

(a) Parallel plane cutting (b) Perpendicular plane cutting

Fig. 4 Section cutting of 3D PCD

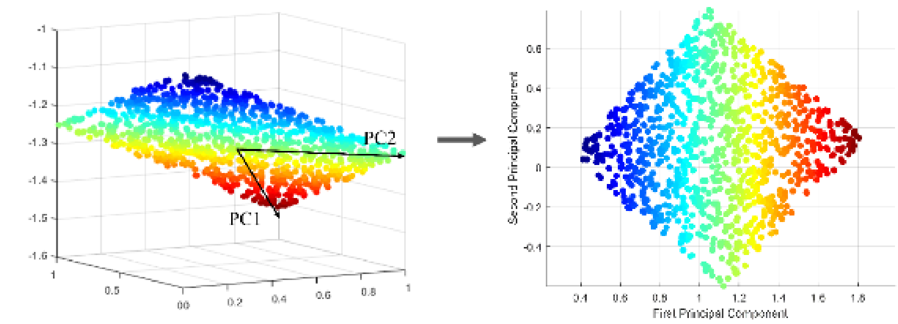

(a) Original data space (b) PCA reduced space

Fig. 5 Conversion of 3D PCD to 2D raster image

planes, respectively. From the parallel plane cutting in Fig. 4(a), one can estimate the length and spacing of the reinforcing bars. On the other hand, when the bars are cut perpendicularly to their longitudinal axis as shown in Fig. 4(b), the diameter of the bars can be estimated from each cross-section.

The thinly sliced PCD can be converted to 2D raster images by conducting principal component analysis (PCA) in MATLAB. PCA is a well-known dimensionality reduction technique, allowing data to be represented in a lower dimension while retaining their major characteristics. Fig. 5 illustrates how PCA reduces the dimensionality of a large dataset from 3D to 2D. Through three perpendicular principal components, actual scale information of the point cloud can be preserved after the conversion. Furthermore, PCA is set to return a 2D image in a binary (black and white) format which is more computationally efficient and advantageous for image processing.

2.3 2D ımage processing

Detailed analysis of reinforcing bar information is carried out through image processing in MATLAB. Herein, analysis operation is divided into two parts, Module 1 and Module 2, depending on the type of information. Before the main analysis, morphology operations are preceded on 2D binary raster images to clearly delineate the binary regions and remove noise. The basic rules of morphology operations include erosion and dilation, which process corresponding pixels based on neighboring pixels in a binary image composed of 0 and 1. In dilation, if any neighboring pixel has a value of 1, the corresponding pixel is set to 1, which makes the object more distinct and can fill small holes. Conversely, erosion sets a pixel to 0 if any neighboring pixel is 0, which helps remove fine lines from the binary image, thus reducing noise.

Fig. 6 shows an example of applying the morphology

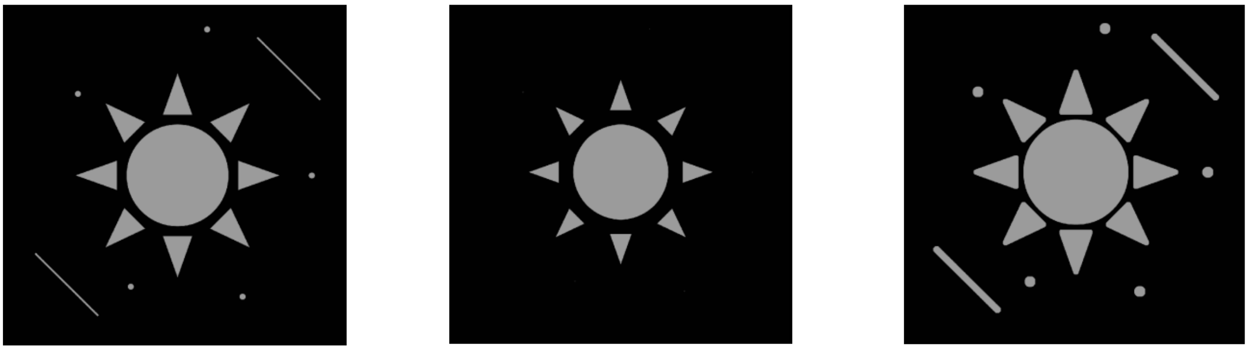

(a) Original binary image (b) Erosion (c) Dilation

Fig. 6 Morphology operations

operations to an example binary image. In this stage, morphology dilation was used to fill any empty spaces inside the reinforcing bars after conversion, and morphology erosion was utilized to remove external noise from around the reinforcing bars.

2.3.1 Module 1

Module 1 is intended to obtain the length of each bar and spacing between adjacent bars. From 2D binary images obtained from the parallel plane section cutting (see Fig. 4(a)), reinforcing bars in different directions (e.g., X and Y directions) are recognized and distinguished on the 2D plane, using a median filter. This filter arranges the surrounding pixels in order of size, and takes the middle value, which is commonly used for noise removal. By setting a threshold, a range recognized as noise can be defined. For the binary images of reinforcing bars, thresholds are set differently for the X and Y directions, respectively, identifying the bars in one direction as noise, thereby obtaining images of the bars in the remaining direction. After the recognition of the bars, each bar is labeled and its center line is drawn, using MATLAB's built-in functions, 'bwlabel' and 'regionprops', respectively. The center lines are used to estimate the length of the corresponding bars. Subsequently, 2D convolution between two arrays is performed in MATLAB, using a built-in function 'conv2' to locate the intersecting region of the two bars and find the center point of the region to calculate the distance (i.e., spacing) between neighboring centers.

2.3.2 Module 2

In Module 2, the diameter of reinforcing bars can be found by processing 2D binary images obtained from the perpendicular plane section cutting (see Fig. 4(b)). Circles are detected from cross-sections of the bars, and center point and diameter (or radius) are identified for each circle. Given the irregularities of actual cross-sections of the bars, there is a high potential for errors in diameter estimation. To minimize the errors, the Hough transform algorithm (Yuen *et al.* 1990) is used. A circle can be mathematically represented by Eq. (4).

$$(x-a)^2+(y-b)^2=r^2 \tag{4}$$

where a and b are the coordinates for a center point of the circle, respectively, and r is the radius. This algorithm finds combinations of (a, b, r) that satisfy the equation of the circle for all points in the image. In MATLAB, a built-in function 'imfindcircles' uses a 3D array for each combination to locate the position with the highest accumulation, from which the center and radius of the circle are estimated. Typically, this algorithm is used to detect geometric shapes such as lines and circles in images. It determines whether pixels in a binary image lie on a circle, allowing for the estimation of the circle's center and radius. Similarly, in Module 2, the center-to-center spacing of reinforcing bars can be obtained using the center of the circles. By identifying the circles and their centers, the distances between the centers can be calculated to determine the center-to-center spacing.

3. Experimental validation

The feasibility and effectiveness of the proposed technique was experimentally validated through two example cases. The grid-type reinforcing bar assembly and the reinforcing bar cage for the RC beam are used in the first and second examples, respectively. From the two cases, information including the length of reinforcing bars and spacing between adjacent bars is obtained.

3.1 Example 1: Reinforcing bar grid

3.1.1 3D modeling and 2D image processing

Fig. 7 shows the details of small-scale grid-type reinforcing bar assembly used in Example 1. Considering the result of the previous study by Kim *et al.* (2021), which highlighted the limitations of using a laser scanner for detecting reinforcing bars with small diameters, this assembly was selected to check whether it is possible to distinguish between small diameters, specifically D10 and D13 bars. The dimensions of the assembly are 600 mm by 375 mm, with the center-to-center bar spacing of 200 mm horizontally and 100 mm vertically. Four 20-mm thick spacers were used to support the specimen above the floor surface. Video shooting was conducted in an indoor laboratory with a marker placed under the specimen (see Fig. 7(b)), which was used to align reference points during the image matching in Metashape. Approximately 100 image frames were extracted from the video footage.

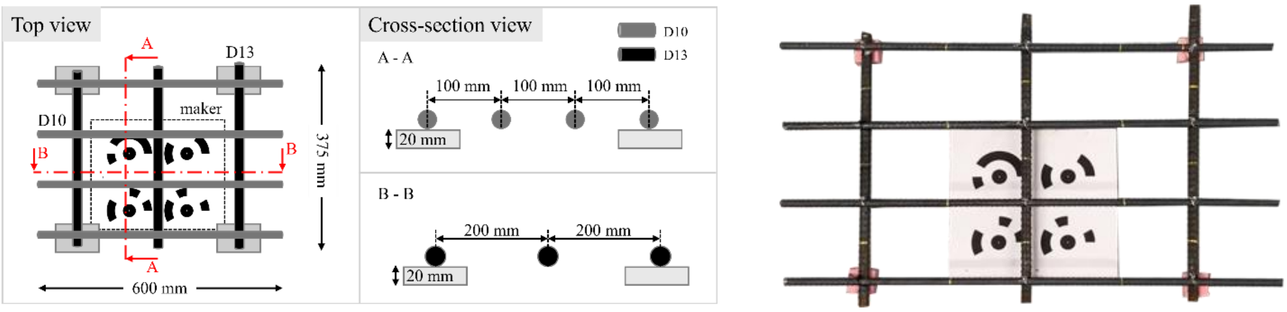

(a) Dimensions (b) Specimen from top view

Fig. 7 Reinforcing bar grid specimen

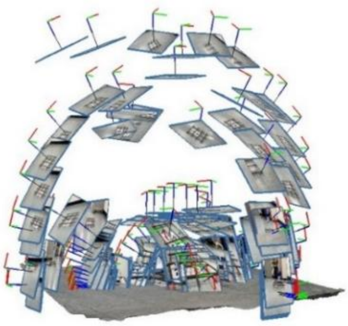

Fig. 8 Images of the reinforcing bar grid specimen

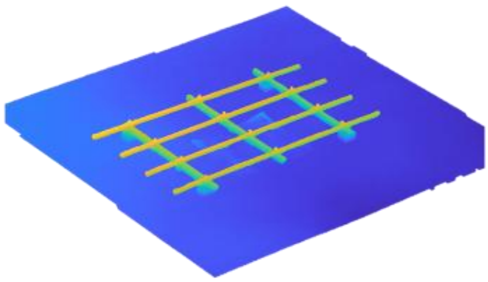

(a) Original point cloud

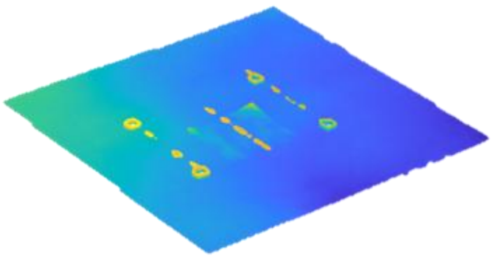

(b) Plane detection

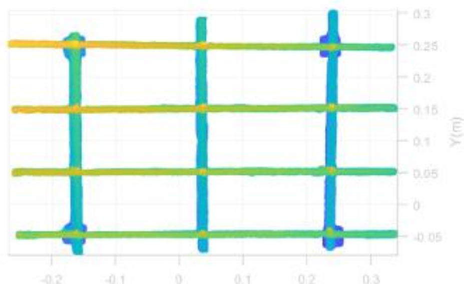

(c) Reinforcing bar extraction

Fig. 9 Separation of the reinforcing bars through plane detectiongy operations

Fig. 8 displays the extracted images with their relative locations around the target object. From these image data, 3D PCD were generated using Metashape. The raw 3D PCD imported into MATLAB went through the plane detection process. Fig. 9 illustrates how the floor surface was removed to separate the reinforcing bar model. After the conversion to 2D binary raster images, the analysis operation in Module 1 and Module 2 followed. Fig. 10 depicts how the length and spacing of the reinforcing bars were estimated from Module 1. The 3D PCD of the specimen was cut by the parallel plane as shown in Fig. 4(a), and a resulting 2D binary raster image was obtained. The horizontal and vertical bars were then recognized and separated as seen in Fig. 10(a). Through the 2D image processing, the information including the length, center-to-center spacing was numerically presented in Fig. 10(b) and 10(c). From the perpendicular plane cutting shown in Fig. 4(b), Module 2 detected the cross-section of the bars through the circle detection and provided numerical values of the bar diameter in Fig. 11. By computing the distance between the center point of the circles, the spacing between the bars can be estimated as well in Module 2.

3.1.2 Assessment

The adequacy of the placement of reinforcing bars can be assessed by comparing the estimated information with reference values determined in the structural design process. In the current study, the accuracy of the information obtained from the examples was verified by comparing it with the actual measured values obtained through Module 1, as presented in Tables 1 and 2. Both Module 1 and Module 2 can measure the center-to-center spacing of the reinforcing bars. However, for consistency with the actual measurement locations, the estimated values from Module 1 were used for Specimen 1. The bar and spacing IDs can be found in Fig. 10(a). The actual length and spacing of the bars were measured using a ruler, and the actual diameter was measured using vernier calipers.

First, Table 1 presents the actual and estimated lengths of the seven reinforcing bars, and corresponding errors. The proposed technique showed overall satisfactory performance in the length estimation for all seven bars,

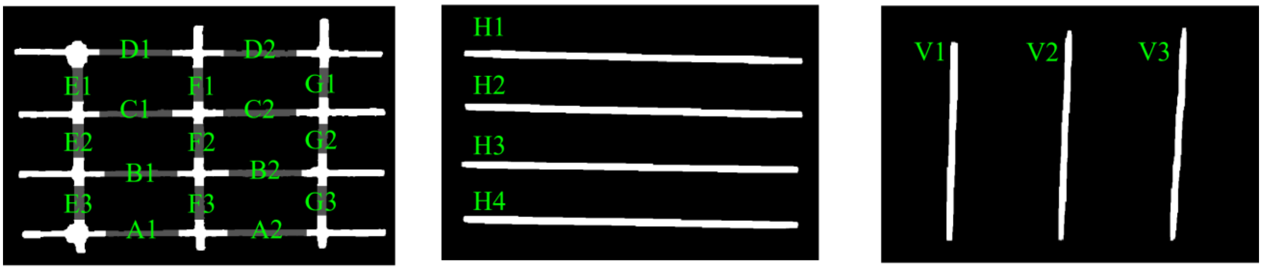

(a) 2D images of horizontal and vertical reinforcing bars

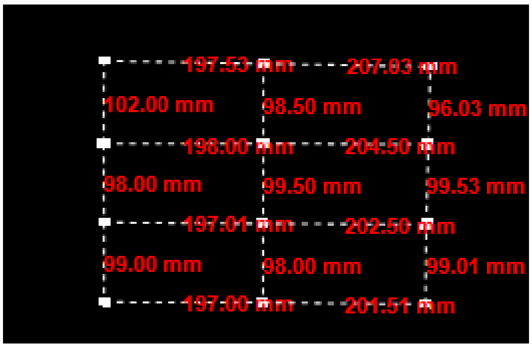

(b) Center-to-center spacing

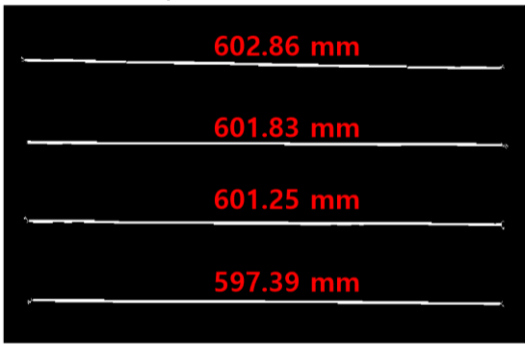

(c) Length (horizontal bars)

Fig. 10 Length and spacing estimation in Example 1 (Module 1)

(a) Center-to-center spacing

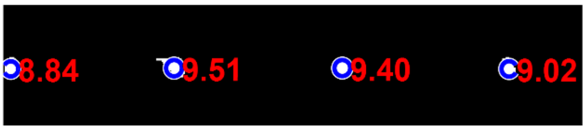

(b) Diameter

Fig. 11 Spacing and diameter estimation in Example 1 (Module 2)

Table 1 Evaluation of length of the reinforcing bars (Example 1)

Bar Type	Bar ID	Actual Value (mm)	Estimation (mm)	Mean Error (%)
D10 (horizontal)	H1	597	597.39	0.15
	H2	600	601.25	
	H3	600	601.83	
	H4	603	602.86	
D13 (vertical)	V1	350	350.96	0.30
	V2	370	370.15	
	V3	375	377.19	

ensuring the mm-level precision. The error in length ranged about 0.1~2.2 mm which corresponded to 0.04~0.58% of the total bar length. In Table 1, the D13 bars exhibited a slightly higher mean error (0.3%) compared to the D10 bars. The results of detecting the center-to-center spacing of the bars are summarized in Table 2. For the 200 mm and 100 mm spacings, the estimation errors as high as 7.03 mm were reported. However, the average errors were found to be only 1.63% and 1.65% for the horizontal and vertical bars, respectively, demonstrating that the effective and precise information acquisition can be achieved.

The diameter of the D10 and D13 bars were estimated at locations shown in Fig. 12. Given the irregular cross-sections of the bars along the length and their small sizes, there is a high probability of error occurrence. For more accurate and consistent diameter estimation, the diameter of horizontal bars (D10) was measured at two points, and that of vertical bars (D13) was measured at three points, after which the averages are compared in Fig. 13. For the purpose of distinguishing the size of the bars (i.e., D10 or D13) from the estimated values, the allowable tolerance range of the diameter was set. The lower and upper bounds of the range was selected as mean values of the nominal diameters of two neighboring bars. For example, for the D10 (9.53 mm diameter) bar positioned between D8 (7.94 mm diameter) and D13 (12.7 mm diameter) bars, the range of 8.74~11.11 mm was set by calculating the mean nominal diameter of the D8 and D10 bars (lower bound), and D10 and D13 bars (upper bound), respectively.

On the other hand, the allowable tolerance range of D13

Table 2 Evaluation of center-to-center spacing of the reinforcing bars (Example 1)

Bar Type	Bar ID	Actual Value (mm)	Estimation (mm)	Mean Error (%)
D10 Bar (horizontal)	A1	200	197	1.63
	A2		201.51	
	B1		197.01	
	B2		202.5	
	C1		198	
	C2		204.5	
	D1		197.53	
	D2		207.03	
D13 Bar (vertical)	E1	100	102	1.65
	E2		98	
	E3		99	
	F1		98.5	
	F2		99.5	
	F3		98	
	G1		96.03	
	G2		99.53	
	G3		99.01	

(a) D10 bar (horizontal) (b) D13 bar (vertical)

Fig. 12 Locations of reinforcing bar diameter estimation

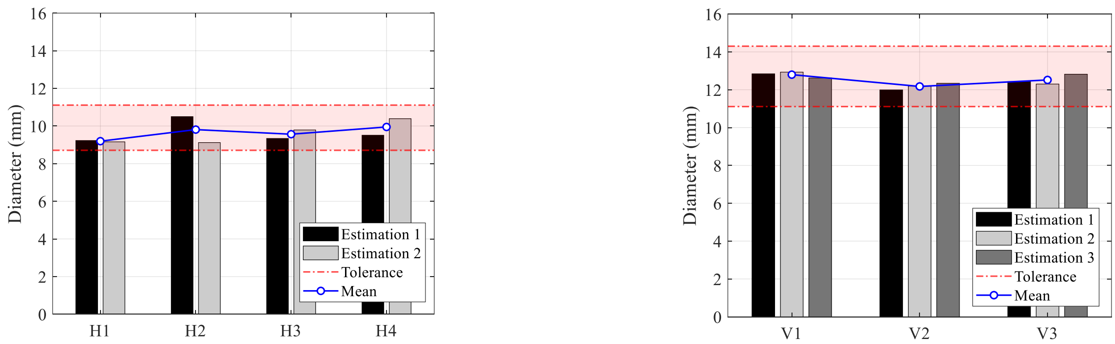

(a) D10 bar (horizontal) (b) D13 bar (vertical)

Fig. 13 Estimation of reinforcing bar diameter in Example 1 (Module 2)

bar was set as 11.12~14.3 mm considering D10 and D16 (15.9 mm diameter). For the comparison, the nominal diameter of the steel bars specified in KS D3504:2021 (Korea Agency for Technology and Standards 2021) was used. The results in Fig. 13 show that all the estimated diameters were within the allowable tolerance ranges, confirming that the technology effectively classified the small diameters of D10 and D13 bars.

3.2 Example 2: Reinforcing bar cage for RC beam

3.2.1 3D modeling and 2D ımage processing

The reinforcing bar grid in Example 1 demonstrated the high accuracy estimation with a simple configuration,

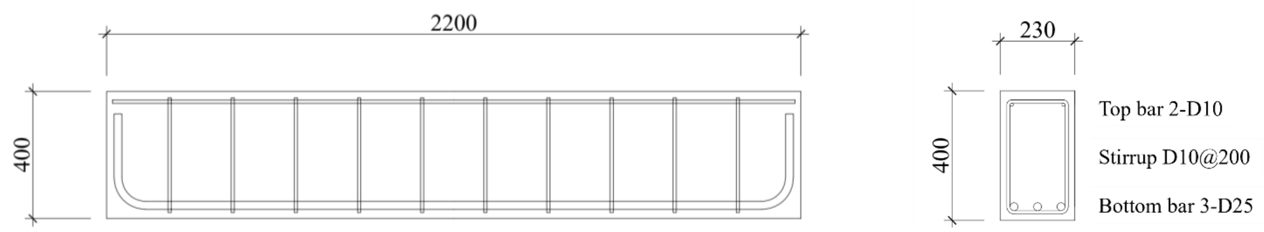

(a) Elevation (b) Cross-section

Fig. 14 Drawing of a RC beam (units in mm)

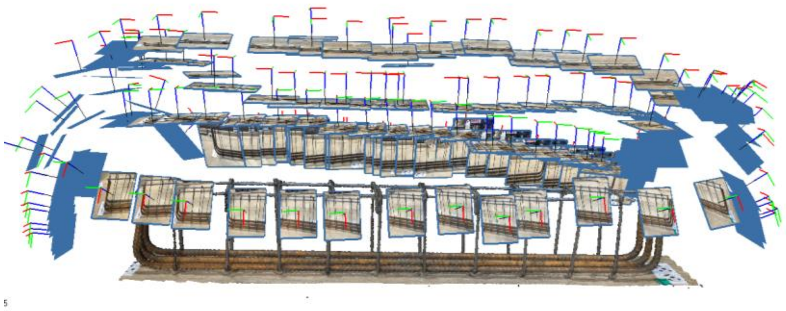

Fig. 15 Extracted image frames

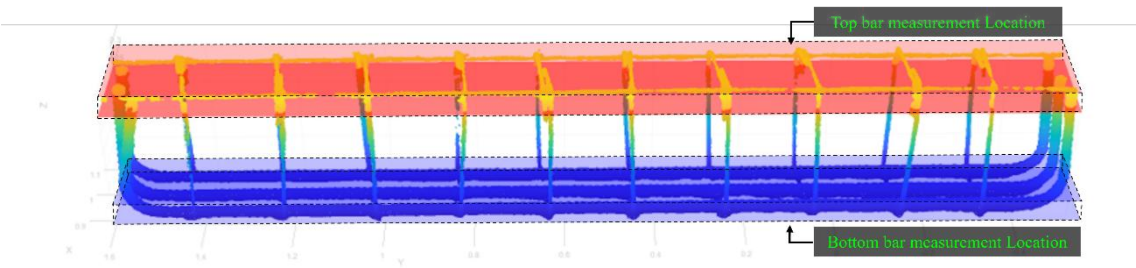

(a) Measurement locations

(b) Numbering (ID) of top longitudinal bars and stirrups

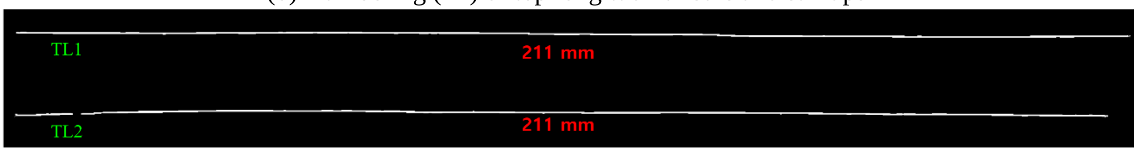

(c) Length of top longitudinal bars

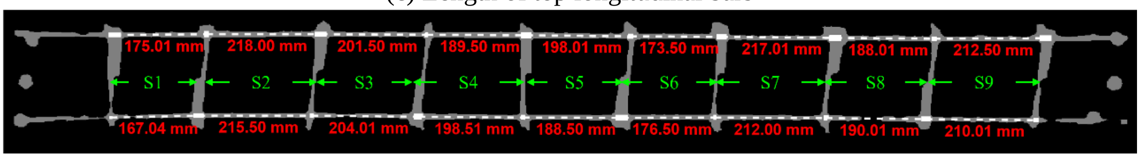

(d) Center-to-center spacing of stirrups

Fig. 16 Length and spacing estimation in Example 2 (Module 1)

showcasing the effectiveness of the I-ARMI technique. To evaluate the accuracy of the developed technology for more realistic and complex configurations, a reinforcing bar cage for the RC beam was fabricated as shown in Fig. 14 The dimensions of the beam are 2200 mm×400 mm×230 mm, using D10 and D25 bars as longitudinal reinforcements at the top and bottom of the section, respectively. For stirrups, D10 bars were provided at every 200 mm along the length of the beam. The video shooting was conducted for the reinforcing bar cage outdoors, using the identical iPhone SE. The video length was approximately 2 minutes. Fig. 15 shows the 3D PCD generated from the 100 image frames.

In Figs. 16 and 17, the information estimated from Module 1 and Module 2 is graphically represented,

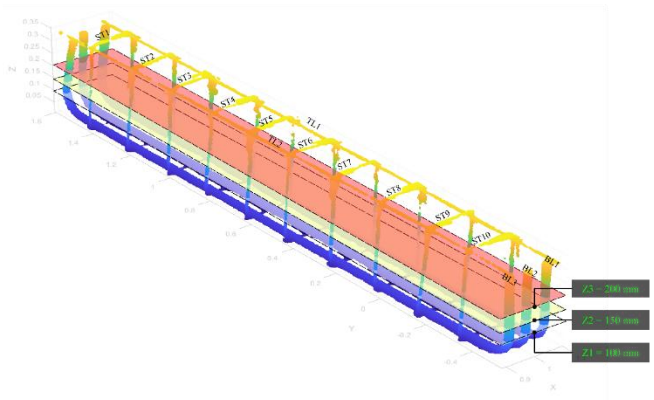

(a) Measurement locations

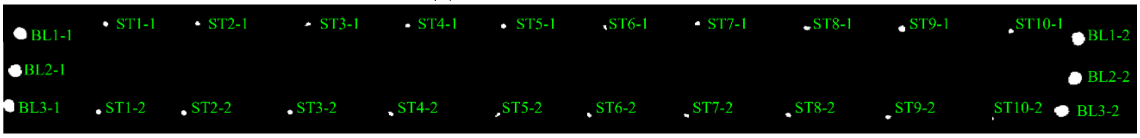

(b) Numbering (ID) of cross-sections of bottom longitudinal bars and stirrups

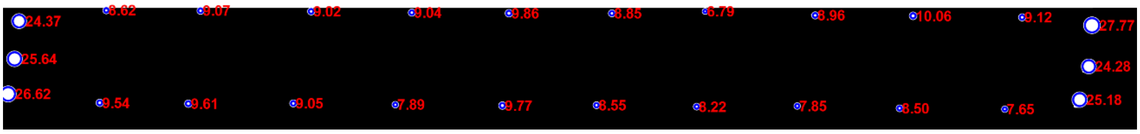

(c) Diameter of bottom longitudinal bars and stirrups

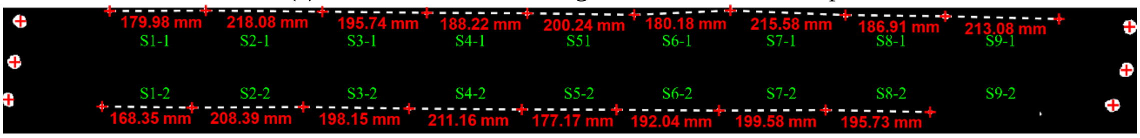

(d) Center-to-center spacing between stirrups

Fig. 17 Diameter and spacing estimation in Example 2 (Module 2)

Table 3 Length of longitudinal bars in Example 2

Bar Type	Bar ID	Actual Value (mm)	Estimation (mm)	Error (%)	Mean Error (%)
D10 (top)	TL1	216	211	2.31	2.34
	TL2	216	211	2.36	
D25 (bot.)	BL1	216	208.2	3.61	3.81
	BL2		207.8	3.80	
	BL3		207.3	4.03	

respectively. Fig. 16 shows the length and center-to-center spacing of the longitudinal and transverse reinforcement. To capture the information at specific locations, 2D images are obtained at different heights by setting the vertical axis (Z-axis) range of the original point cloud. Fig. 16(a) shows the measurement locations in Module 1. To obtain the length information of the longitudinal reinforcing bars, regions containing the top and bottom bars were separately designated. Fig. 17(a) indicates the measurement locations in Module 2. Considering the variability of the cross-section of the bars, the diameter was estimated at three different locations for each bar by setting the Z-axis coordinate as 0.1 m, 0.15 m, and 0.2 m in the 3D point cloud model. The center-to-center spacing of the stirrups was estimated in Module 2 as well at Z3 (200 mm) location.

3.2.2 Assessment

Table 3 provides the length of the longitudinal bars detected in Module 1 and compares them with actual measured values. The two top longitudinal bars and three bottom longitudinal bars are denoted as TB and BL, respectively, in Table 3. The average error rate for the top bars was 2.34% while the bottom bars showed a higher error rate of 3.81%. Compared to the top bars, the bottom bars were found to have relatively shorter estimated length because of their bended area (i.e., 90° hook) near the base of the beam (see Fig. 16(a)). Accordingly, the bottom bars had the higher error rate.

Table 4 compares the actual and estimated values of the center-to-center spacing of the stirrups obtained through Module 2. The spacing of the stirrups was estimated along the two imaginary (dashed) lines as shown in Fig. 17(d). The average error rate for S1-1 to S9-1 was 1.58%, while that for S1-2 to S9-2 was 2.01%. The segments with the

Table 4 Center-to-center spacing of stirrups in Example 2

Spacing ID	Actual Value (mm)	Estimation (mm)	Error (%)	Mean Error (%)
S1-1	180	179.98	0.01	
S2-1	220	218.08	0.87	
S3-1	200	195.74	2.13	
S4-1	190	188.22	0.94	
S5-1	205	200.24	2.32	1.58
S6-1	185	180.18	2.61	
S7-1	215	215.58	0.27	
S8-1	195	186.91	4.15	
S9-1	215	213.08	0.89	
S1-2	170	168.35	0.97	
S2-2	215	208.39	3.07	
S3-2	200	198.15	0.92	
S4-2	210	211.16	0.55	
S5-2	185	177.17	4.23	2.01
S6-2	195	192.04	1.52	
S7-2	205	199.58	2.64	
S8-2	200	195.73	2.14	
S9-2	210	-	-	

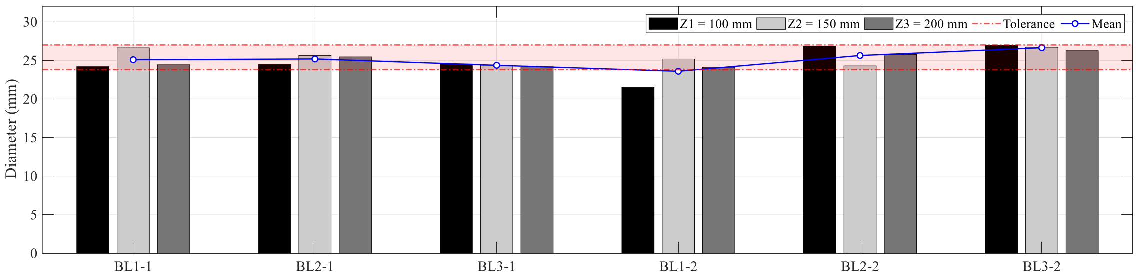

Fig. 18 Diameter estimation of bottom longitudinal bars (D25)

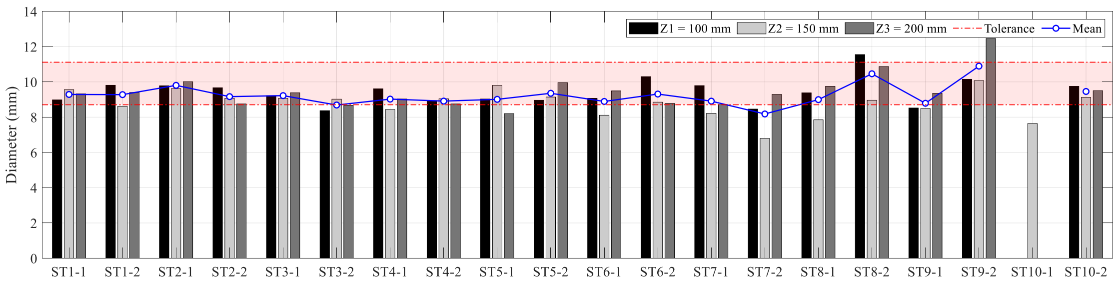

Fig. 19 Diameter estimation of stirrups (D10)

highest error rates were S8-1 and S5-2, showing error rates of 4.15% and 4.23%, respectively. Additionally, S9-2 could not be detected due to the improper detection of reinforcing bar ST10-2 (see Fig. 17(b)). The average center-to-center distances for each segment were 193.82 mm and 197.56 mm, with a difference of approximately 2~6 mm from the design value of 200 mm, demonstrating the high accuracy and reliability of this method in reinforcing bar placement inspection. When verifying the length and spacing of the steel bars, all detected values were slightly shorter than the actual measurements. This indicates the potential existence of systematic bias in the detection process. Factors such as the resolution of the point cloud and the overlapping of steel bars may contribute to these errors.

Figs. 18 and 19 depict the diameter estimation results for the bottom longitudinal bar (D25) and stirrups (D10), respectively. The allowable tolerance ranges were determined based on the nominal diameters specified in KS

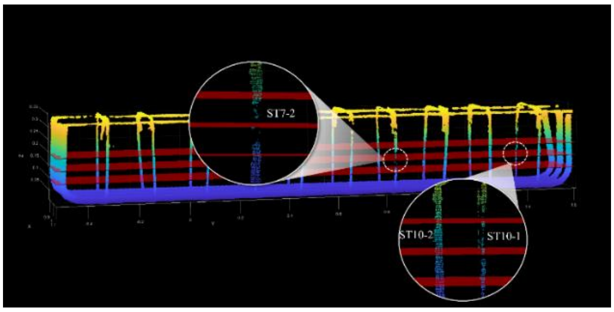

Fig. 20 Enlarged 3D Point Cloud Model and Stirrup Images at Locations ST7-2 and ST10-1

D3504:2021 construction standards (Korea Agency for Technology and Standards 2021) as described earlier. For D25 bar, the range was set between 23.8 mm and 27 mm, while for D10 bar, it was set between 8.74 mm and 11.11 mm. In Fig. 18, it was observed that the diameter of D25 bars exhibited some variability depending on the Z-axis locations but on average the estimated values fell within the allowable tolerance range. On the other hand, for the D10 bars, the average estimations met the allowable tolerance range at the 18 out of 20 locations as shown in Fig. 19. It is clearly seen that the diameter estimated at the locations ST7-2 and ST10-1 fell far short of the criterion. Especially, at the location ST10-1, the bar was not even detected at two points (i.e., Z1=100 mm and Z3=200 mm).

3.2 Discussion

In this study, approximately 100 image frames were used under laboratory conditions to generate a 3D point cloud model, which showed sufficient performance in detecting the length, diameter, and center-to-center spacing of reinforcing bars. However, considering the complex reinforcing bar arrangements and inconsistent lighting conditions in real construction sites, it is necessary to secure a greater number of images, and additional experiments are required to determine the optimal number of images. Additionally, applying interpolation techniques to compensate for data loss that may occur during image acquisition could be an effective solution.

Future research should focus on developing an algorithm to calculate the intersection angle based on the centerlines of the reinforcing bars and detecting rebar hooks automatically through curvature analysis and pattern recognition of the 3D point cloud model. Furthermore, by applying deep learning-based rebar shape recognition technology, it is expected that precise detection can be achieved even in complex reinforcement environments.

To figure out the causes of the inaccurate diameter estimation, the 3D point cloud model was examined closely. The 3D point cloud model with enlarged images of the stirrups at the locations ST7-2 and ST10-1 on the surface at Z1, Z2, and Z3 is provided in Fig. 20. It is obviously seen that the 3D point cloud model at the corresponding locations was disconnected and partially disappeared. Such poor modeling was found to be attributed to the low-quality images extracted from the video. Fig. 21 shows the improperly captured and out-of-focus images of the stirrups used in the generation of 3D point cloud model. Accordingly, subsequent image processing and diameter estimation steps also appeared to yield significant errors.

Fig. 21 Low-quality image frames of stirrups extracted from the video

Several factors contributed to this issue. The first is the shooting environment and lighting conditions. When the lighting is inconsistent, reflections on the surface of the rebar can obscure its boundaries, making it difficult to distinguish rebar outlines. Shadows or variations in brightness may reduce the contrast of the image, further degrading the edge clarity. The second factor is focus-related problems. Some images were out of focus, resulting in blurred reinforcing bar shapes and data loss in the 3D point cloud model. If the camera shakes during shooting or the focal distance is not maintained consistently, image quality deteriorates and the model accuracy may be reduced. The third factor is the limitation of the image extraction method. This study used frame extraction from video recording, and some frames were saved in lower resolution. Depending on the camera movement speed or shooting conditions, specific frames may become blurred or distorted, making it more difficult to construct an accurate 3D model.

To address these issues, it is recommended to ensure uniform lighting conditions, utilize diffused lighting to minimize surface reflections, adopt fixed-focus settings during image capture, and maintain an image overlap ratio between 60% and 80%. Additionally, future research should consider implementing interpolation techniques to compensate for data loss during the 3D point cloud generation process and developing machine learning-based automatic recognition algorithms to ensure reliable model construction in complex on-site environments.

4. Conclusions

In this study, a new automatic reinforcement modeling and inspection technique was developed using photogrammetry to overcome the limitations of traditional structural inspection methods. The proposed technique uses smartphone cameras for acquisition of images and construction of 3D point cloud models, presenting a cost-effective alternative for construction sites. The performance and feasibility of the technique was validated on the laboratory-scale reinforcing bar grid and cage specimens with a satisfactory accuracy. The following is a summary of the most important findings of the current study:

• Through the framework of I-ARMI technique, a 3D point cloud model can be effectively established by assembling multiple images of a target subject, and important information including length, spacing, and diameter of steel reinforcing bars can be acquired through CV and image processing.

• The proposed method demonstrated high accuracy on the laboratory-scale reinforcing bar grid specimen, showing 99% accuracy for bar length and over 98% for bar spacing. Especially, it successfully detected the diameters of small diameter bars (D10 and D13) with an average error of 0.27 mm.

• When applied to the reinforcing bar cage, the proposed technique achieved about 97% accuracy in estimating the length and center-to-center spacing of reinforcing bars. The diameter estimation yielded the accurate results for all D25 bars. The diameter of D10 stirrups was within the acceptable range at 18 out of 20 locations.

• Although the I-ARMI technique has been validated in a laboratory environment, additional improvements such as drone integration and deep learning-based automation models are required for large-scale construction applications. This will enable rapid image data collection for large structures and allow for broader detection of reinforcing bars.

The proposed technique demonstrated satisfactory performance under relatively well-controlled laboratory conditions. However, since construction sites are highly complex environments, detection accuracy may decrease due to issues such as out-of-focus, blurry, or irrelevant images, which can significantly degrade the quality of the 3D model. Future studies should focus on incorporating advanced techniques such as machine learning to enhance the automatic identification of target reinforcing bars and the completeness of the 3D model. In addition, because the required number of images may vary depending on the complexity of the reinforcement configuration, future research will include experiments aimed at determining the optimal number of images.

Acknowledgments

This work was supported by the National Research Foundation of Korea (NRF) grant funded by the Korea government (MSIT) (No. NRF-2020R1A2C3005687) and was supported by a Korea University grant.

References

Alaloul, W.S., Qureshi, A.H., Musarat, M.A. and Saad, S. (2021), "Evolution of close-range detection and data acquisition technologies towards automation in construction progress monitoring", *J. Build. Eng.*, **43**, 102877. https://doi.org/10.1016/j.jobe.2021.102877.

Balbin, J.R., Hortinela IV, C.C., Garcia, R.G., Baylon, S., Ignacio, A.J., Rivera, M.A. and Sebastian, J. (2017), "Pattern recognition of concrete surface cracks and defects using integrated image processing algorithms", *Second International Workshop on Pattern Recognition*, Singapore, Singapore, May.

Cavaco, E., Pimenta, R. and Valença, J. (2019), "A new method for corrosion assessment of reinforcing bars based on close-range photogrammetry: Experimental validation", *Struct. Concrete*, **20**(3), 996-1009. https://doi.org/10.1002/suco.201800196.

Cheng, Y.J., Zheng, W.L. and Qiu, W.G. (2023), "Reconstruction of tunnel lining rebars from terrestrial laser scanning data", *Struct. Concrete*, **24**(1), 563-582. https://doi.org/10.1002/suco.202200897.

Hidayat, B.A., Hsiao, F.P., Hu, H.T., Lie, H.A., Pita, P. and Haryanto, Y. (2020), "Seismic performance of non-ductile detailing RC frames: An experimental investigation", *Earthq. Struct.*, **19**(6), 485-498. https://doi.org/10.12989/eas.2020.19.6.485.

Im, C.R., Kim, S., Mun, J.H., Yang, K.H. and Sim, J.I. (2025), "Seismic performance of concrete-filled hollow precast concrete columns with prefabricated inner mold", *Steel Compos. Struct.*, **54**(4), 331-344. https://doi.org/10.12989/scs.2025.54.4.331.

Jeon, J.S., Kim, H.J. and Shim, D.S. (2018), "MSAC/PROSAC Fusion algorithm to enhance SURF performance for visual SLAM", *Information and Control Symposium*, Pyeongchang, Gangwon, Korea, October.

Kim, M.K., Thedja, J.P.P. and Wang, Q. (2020), "Automated dimensional quality assessment for formwork and rebar of reinforced concrete components using 3D point cloud data", *Automat. Constr.*, **112**, 103077. https://doi.org/10.1016/j.autcon.2020.103077.

Kim, M.K., Thedja, J.P.P., Chi, H.L. and Lee, D.E. (2021), "Automated rebar diameter classification using point cloud data based machine learning", *Automat. Constr.*, **122**, 103476. https://doi.org/10.1016/j.autcon.2020.103476.

Korea Agency for Technology and Standards (2021), KS D 3504: Steel Bars for Concrete Reinforcement, Korea Standards and Certifications, Seoul, Korea.

Lee, J.H. and Park, S.O. (2019), "Machine learning-based automatic reinforcing bar image analysis system in the internet of things", *Multimedia Tools Appl.*, **78**(3), 3171-3180. https://doi.org/10.1007/s11042-018-5984-7.

Luo, H., Lin, L., Chen, K., Antwi-Afari, M.F. and Chen, L. (2022), "Digital technology for quality management in construction: A review and future research directions", *Dev. Built Environ.*, **12**, 100087. https://doi.org/10.1016/j.dibe.2022.100087.

Mahamid, M., Bilal, K. and Tort, C. (2024), "Behavior and design of multi-sided composite sections", *J. Struct. Integr. Maint.*, **9**(1), 2267329. https://doi.org/10.1080/24705314.2023.2267329.

Masiero, A. (2017), "Photogrammetric 3D reconstruction in Matlab: development of a free tool", *Int. Arch. Photogramm. Remote Sens. Spat. Inf. Sci.*, **XLII-2/W8**, 141-145. https://doi.org/10.5194/isprs-archives-XLII-2-W8-141-2017.

Pleansamai, K. and Chaiyasarn, K. (2019), "M-estimator sample consensus planar extraction from image-based 3D point cloud for building information modelling", *GEOMATE J.*, **17**(63), 69-76. https://doi.org/10.21660/2019.63.09667.

Qureshi, A.H., Alaloul, W.S., Hussain, S.J., Murtiyoso, A., Saad,

S. and Oad, V.K. (2022), "Evaluation of 3D model of rebar for quantitative parameters", *Int. Arch. Photogramm. Remote Sens. Spat. Inf. Sci.*, **48**, 215-220. https://doi.org/10.5194/isprs-archives-XLVIII-2-W1-2022-215-2022.

Remondino, F. (2011), "Heritage recording and 3D modeling with photogrammetry and 3D scanning", *Remote Sens.*, **3**(6), 1104-1138. https://doi.org/10.3390/rs3061104.

Shen, Z., Tang, P., Kanaan, O. and Cho, Y. (2013), "As-built error modeling for effective 3D laser scanning on construction sites", *2013 ASCE Workshop of Computing in Civil Engineering*, Los Angeles, CA, USA, June.

Shin, Y., Heo, S., Han, S., Kim, J. and Na, S. (2021), "An image-based steel rebar size estimation and counting method using a convolutional neural network combined with homography", *Build.*, **11**(10), 463. https://doi.org/10.3390/buildings11100463.

The MathWorks Inc. (2023), MATLAB Version: 9.14.0 (R2023a), The MathWorks Inc., Natick, MA, USA.

Torr, P.H.S. and Zisserman, A. (2000), "MLESAC: A new robust estimator with application to estimating image geometry", *Comput. Vision Image Understand.*, **78**(1), 138-156. https://doi.org/10.1006/cviu.1999.0832.

Torresani, A. and Remondino, F. (2019), "Videogrammetry vs photogrammetry for heritage 3D reconstruction", *Int. Arch. Photogramm. Remote Sens. Spat. Inf. Sci.*, **XLII-2/W15**, 1157-1162. https://doi.org/10.5194/isprs-archives-XLII-2-W15-1157-2019.

Wang, Q. and Kim, M.K. (2019), "Applications of 3D point cloud data in the construction industry: A fifteen-year review from 2004 to 2018", *Adv. Eng. Informat.*, **39**, 306-319. https://doi.org/10.1016/j.aei.2019.02.007.

Wang, Q., Cheng, J.C. and Sohn, H. (2017), "Automated estimation of reinforced precast concrete rebar positions using colored laser scan data", *Comput. Aid. Civil Infrastr. Eng.*, **32**(9), 787-802. https://doi.org/10.1111/mice.12293.

Yuan, X., Moreu, F. and Hojati, M. (2021), "Cost-effective inspection of rebar spacing and clearance using RGB-D sensors", *Sustainab.*, **13**(22), 12509. https://doi.org/10.3390/su132212509.

Yuan, X., Smith, A., Moreu, F., Sarlo, R., Lippitt, C.D., Hojati, M., Alampalli, S. and Zhang, S. (2023), "Automatic evaluation of rebar spacing and quality using LiDAR data: Field application for bridge structural assessment", *Automat. Constr.*, **146**, 104708. https://doi.org/10.1016/j.autcon.2022.104708.

Yuen, H.K., Princen, J., Illingworth, J. and Kittler, J. (1990), "Comparative study of Hough transform methods for circle finding", *Image Vision Comput.*, **8**(1), 71-77. https://doi.org/10.1016/0262-8856(90)90059-E.

DL